DOI: 10.13009/EUCASS2025-270
11TH EUROPEAN CONFERENCE FOR AERONAUTICS AND SPACE SCIENCES (EUCASS)

Modeling the impact of a supersonic hot gas jet on aluminum sheets for recycling fragmentation

Tetyana Nabokina, **†, and Christian Bach***
** National Aerospace University "Kharkiv Aviation Institute"*
Vadyma Manka St. 17, 61070 Kharkiv, Ukraine
*** Technische Universität Dresden*
Marschnerstrasse 32, 01307 Dresden, Germany
tetyana.nabokina@mailbox.tu-dresden.de – christian.bach1@tu-dresden.de
† Corresponding Author

Abstract
Supersonic jets of combustion products from low-thrust rocket engines are capable of cutting aluminum sheet materials in both melting and non-melting regimes, depending on thermogasdynamic jet parameters, target material properties, and nozzle positioning parameters. This study develops a numerical model to predict temperature and stress fields in the jet–target interaction zone. Simulations are performed using SolidWorks Simulation, based on strength of materials, heat transfer and rocket engine theory. The results confirm that material fragmentation without melting is achievable, reducing energy consumption by ~20 % and demonstrating higher efficiency compared to conventional melting-based cutting.

1. Introduction

The capability to effectively fragment and recycle metallic structures holds critical significance within the framework of In-Situ Resource Utilization (ISRU) strategies, particularly in extraterrestrial environments such as the lunar surface. Efficient fragmentation methods are vital for minimizing energy consumption, reducing logistical burdens from Earth, and maximizing the reuse of available materials during long-term missions and habitat construction on the Moon. Supersonic hot gas jets generated by low-thrust rocket engines offer a promising technological solution for achieving rapid, energy-efficient recycling of aerospace-grade aluminum alloys, aligning with current goals for sustainable exploration and the establishment of permanent lunar bases.
Thermal jet cutting is one of the widely used subtractive manufacturing processes and is extensively applied in industrial practice. Jet energy is utilized in various forms both for precision operations, such as material cutting, coating removal, and material cutting, and for heavy-duty applications, including the dismantling and fragmentation of large-scale structures such as ships, bridges, and buildings, as well as rock breaking in mining industries. Potential thermal methods for the recycling and cutting of large metallic structures have been comprehensively analyzed in recent studies [1].
Preliminary experimental investigations have indicated that the use of supersonic, high-temperature gas jets generated by low-thrust rocket engines represents a promising approach for the fragmentation of aluminum sheet materials. Such jets, with exit velocities around 2000 $m \cdot s^{-1}$ and temperatures ranging from 2000 K to 3000 K, produce heat flux densities sufficient for the fragmentation of high thermal conductivity materials, such as aluminum and copper alloys. This method enables coarse cutting and, with optimal adjustment of the jet parameters, allows material fragmentation without reaching the melting point [2].
Recent years have seen considerable attention devoted to the modeling and experimental investigation of supersonic and hypersonic jets impacting barriers, primarily for the analysis of aerodynamic behavior, acoustic effects, and thermal loads. These studies are critical for the design of durable and efficient landing pads and protective structures.
In the aerospace sector, such jets are of particular interest due to their role in Plume-Surface-Interactions (PSI) with landing surfaces and spacecraft exteriors, where high-velocity exhaust flows can cause significant thermal and mechanical effects. At a smaller scale, the interaction of supersonic jets with aluminum plates studied in this work can be seen as a model of localized jet-induced processes relevant to spacecraft operations during launch and landing.
Jiang et al. [3] examined the characteristics of jet impingement during rocket landings, primarily focusing on flow structure, acoustic phenomena, and total thermal impact on flat surfaces such as soil and concrete pads, including the

DOI: 10.13009/EUCASS2025-270

interaction of normal and inclined jets. Chan et al. [4] employed Reynolds-Averaged Navier-Stokes (RANS) and Large Eddy Simulation (LES) methods to study the behavior of supersonic jets impacting surfaces at various angles and distances, emphasizing the significance of the dimensionless parameter $h \cdot d_n^{-1}$ (where h is the distance from the nozzle exit to the surface, and d_n is the nozzle exit diameter) in governing pressure and heat flux distributions within the stagnation zone. Experimental work by Goldstein et al. [5] further investigated the heat transfer characteristics of jets impinging at different angles, providing empirical correlations for average Nusselt numbers and mapping isocontours of heat transfer coefficients on flat surfaces.

Although extensive research has been conducted on the thermal and aerodynamic effects of jet impingement, most existing studies have primarily addressed heat transfer characteristics, pressure distributions, and surface erosion phenomena, typically assuming the target plate to be rigid and thermally uniform. Investigations such as those by Dairay et al. [6], Martin [7], Zohbi et al. [8], and Cooper et al. [9] have focused on the development of jet-induced flow structures and heat transfer enhancement, without considering the thermal conductivity, deformation, or failure mechanisms of the plate. Experimental studies by Khalifa et al. [10] and Vinze et al. [11] further examined heat transfer behaviors of jets impinging on metallic plates under various thermal and geometric conditions. However, these works emphasized flow dynamics rather than plate degradation or structural failure. Similarly, research by Subramanian et al. [12] explored jet interactions under near-vacuum conditions relevant to lunar environments but concentrated mainly on flow field characterization without addressing destructive material processes.

Thus, despite considerable progress in understanding jet-surface interactions, the specific mechanisms of material fragmentation, structural weakening, and failure under the impact of supersonic, high-temperature jets – particularly in the context of coarse cutting and fragmentation – remain insufficiently studied.

The present study aims to investigate the interaction between supersonic, high-temperature combustion jets and aluminum plates under orthogonal impingement conditions, with a focus on coarse cutting and fragmentation processes relevant to recycling and disposal applications. A finite element (FE) model has been developed to simulate the thermal and mechanical response of the plate material, incorporating temperature-dependent thermophysical properties and dynamic jet loading.

The primary tasks of this study are as follows:

– to develop a coupled thermal–mechanical simulation framework capable of predicting plate failure under supersonic jet impact;
– to identify and characterize different modes of jet–plate interaction, including heat dissipation without damage (radiator mode), surface melting followed by failure (melting + breakdown mode), and direct failure without melting (breakdown mode);
– to evaluate the energy efficiency of the breakdown-based cutting process compared to melting-based fragmentation approaches;
– to establish a basis for optimizing jet and plate parameters for efficient material fragmentation, with potential adaptation to extraterrestrial environments under ISRU strategies.

The outcomes of this research are intended to support the development of advanced, sustainable material processing technologies applicable both on Earth and in future space exploration missions.

The article is organized as follows. Section 2 presents the theoretical background of jet–plate interaction, focusing on the combined solution of thermal and mechanical problems for modeling the elementary cutting (breakdown) process. Section 3 describes the finite element simulation, detailing the developed model that integrates thermal and mechanical analyses within the SOLIDWORKS Simulation 2022 environment. Section 4 discusses the simulation results, demonstrating the effectiveness of the developed model for evaluating parameters relevant to coarse cutting and fragmentation processes.

2. Research Methods

A supersonic jet of combustion products from a low-thrust rocket engine provides a high concentration of energy over a small area. This enables the use of the jet as a non-contact cutting tool for materials with various thermophysical properties, including those commonly employed in spacecraft structures. Under the action of the jet, a narrow cutting zone is formed, while complex physical processes occur within the structure, involving the redistribution of heat transferred from the jet and the generation of mechanical stresses due to the jet's dynamic pressure.

The present study is based on the investigation of heat transfer within the target plate, the analysis of its stress–strain state, and the assessment of material strength, taking into account temperature-dependent changes in physical properties at elevated temperatures.

The following assumptions were made in the analysis of the cutting process:

1. Upon heating by the jet, the plate's temperature increases, leading to a reduction in its strength.
2. The temperature, and consequently the strength of the material, depends on the exposure time of the jet acting on the plate.

DOI: 10.13009/EUCASS2025-270

3. The dynamic (mechanical) loading from the jet is determined by the surface pressure, which in turn depends on the combustion chamber pressure P_k (see Fig. 1).
4. The internal stresses induced by the dynamic pressure of the jet within the material are assumed to remain constant over time.

Preliminary investigations into the processes of thermal jet cutting have shown that the outcome of supersonic high-temperature jet interaction with a plate can vary significantly depending on the jet parameters and the thermophysical properties of the plate. In addition to the well-known regimes namely**,** heating without failure (occurring when the jet intensity is insufficient to cause material destruction, with a typical jet exposure time $\tau_{infl} \approx 8$ s) (see Fig. 2(a)) and melting (characterized by the localized melting of the material in the jet impingement zone) (see Fig. 2(b)) – two additional regimes were identified during the analysis.
The newly identified regimes are:

- melting + breakdown (see Fig. 2(c)), where the front surface of the plate begins to melt under jet exposure, followed by mechanical ejection of the still-solid underlying material from the cutting zone, with no evidence of melting observed on the rear side of the plate;
- breakdown, in which plate failure occurs solely due to thermal weakening and dynamic pressure effects, without reaching the material's melting temperature (see Fig. 2(d)).

These latter two regimes are characteristic of cutting by supersonic jets.

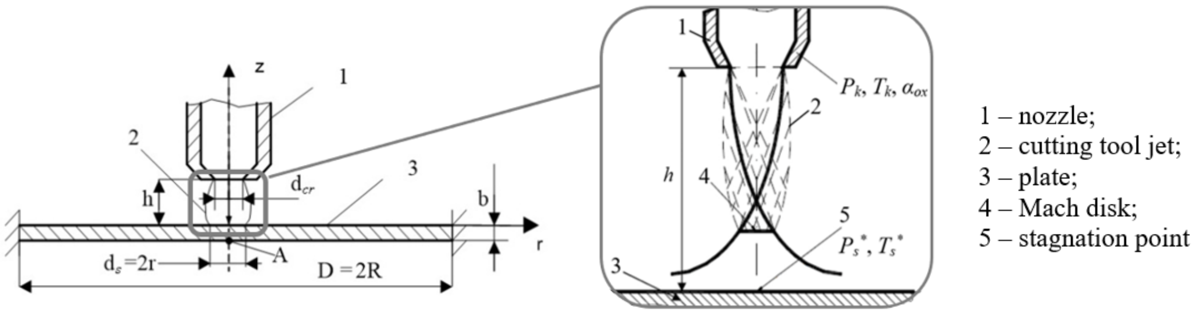

a) b)

Figure 1: Schematic of cutting stage: a) elementary cutting stage; b) distribution of combustion jet parameters within the influence region of the first shock cell ((1.5 – 2) d_n): h – distance between the nozzle and the plate; b – plate thickness; d_{cr} – nozzle diameter; D – plate fixation diameter; d_s – jet diameter upon contact with plate; P_k, T_k, α_{ox} – combustion chamber parameters; P_s^*, T_s^* – stagnation parameters

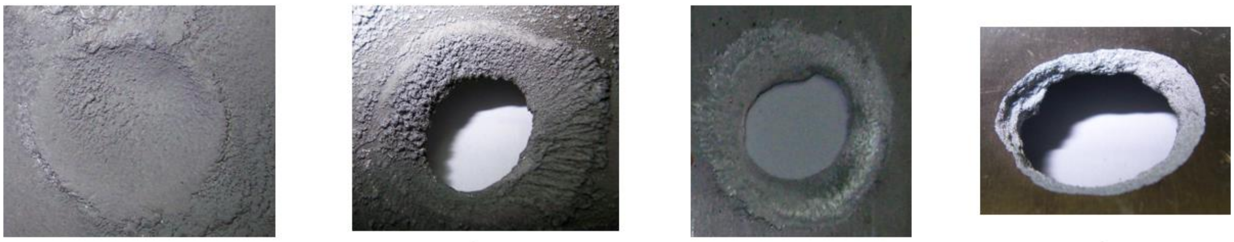

a) b) c) d)

Figure 2: Result of supersonic combustion jet impact on the plate: a) heating without failure; b) melting; c) melting+breakdown; d) breakdown

Previous studies [2] have demonstrated the energy efficiency of the breakdown mode, as the plate does not need to be heated to its melting temperature, thereby eliminating the energy costs associated with phase transition. However, the realization of this mode is possible only under specific conditions related to the local stress state, as well as the thermal and geometric properties of the material.
To investigate the conditions required for the onset of breakdown, a model of the interaction between a stationary jet and a plate was developed. The schematic of an elementary cutting stage is shown in Figure 1. During the analysis, a critical hypothesis was introduced: breakdown is expected to occur at the moment when the maximum internal stress generated by the jet's dynamic pressure σ_r equals the minimum tensile strength $\sigma_u(T)$ of the material at the rear side of the plate along the jet axis (point A, see Fig. 1(a)), provided that the surface temperature of the plate remains below the melting point.
Thus, the breakdown condition at the moment τ (in point A in Fig. 1(a)) can be formulated as:

DOI: 10.13009/EUCASS2025-270

$$\sigma_r^{\ max} = \sigma_u(T)^{min}, \qquad \textbf{(1)}$$

where σ_r – internal stress in the plate caused by the dynamic component of the jet pressure;
$\sigma_u(T)$ – tensile strength of the material as a function of temperature.

Thus, it is necessary to determine the time, required to heat point A to a temperature at which the material's tensile strength equals the internal stresses induced by the jet's dynamic component. This problem was approached in two stages:

1. Analyzing the temperature distribution in a finite-thickness plate exposed to a high-temperature combustion jet over time, along with the corresponding changes in strength.
2. Determining the maximum stresses in the material caused by the jet's dynamical impact on the plate.

The flowchart of the algorithm developed for investigating the cutting process of sheet materials by a supersonic high-temperature jet is presented in Figure 3.

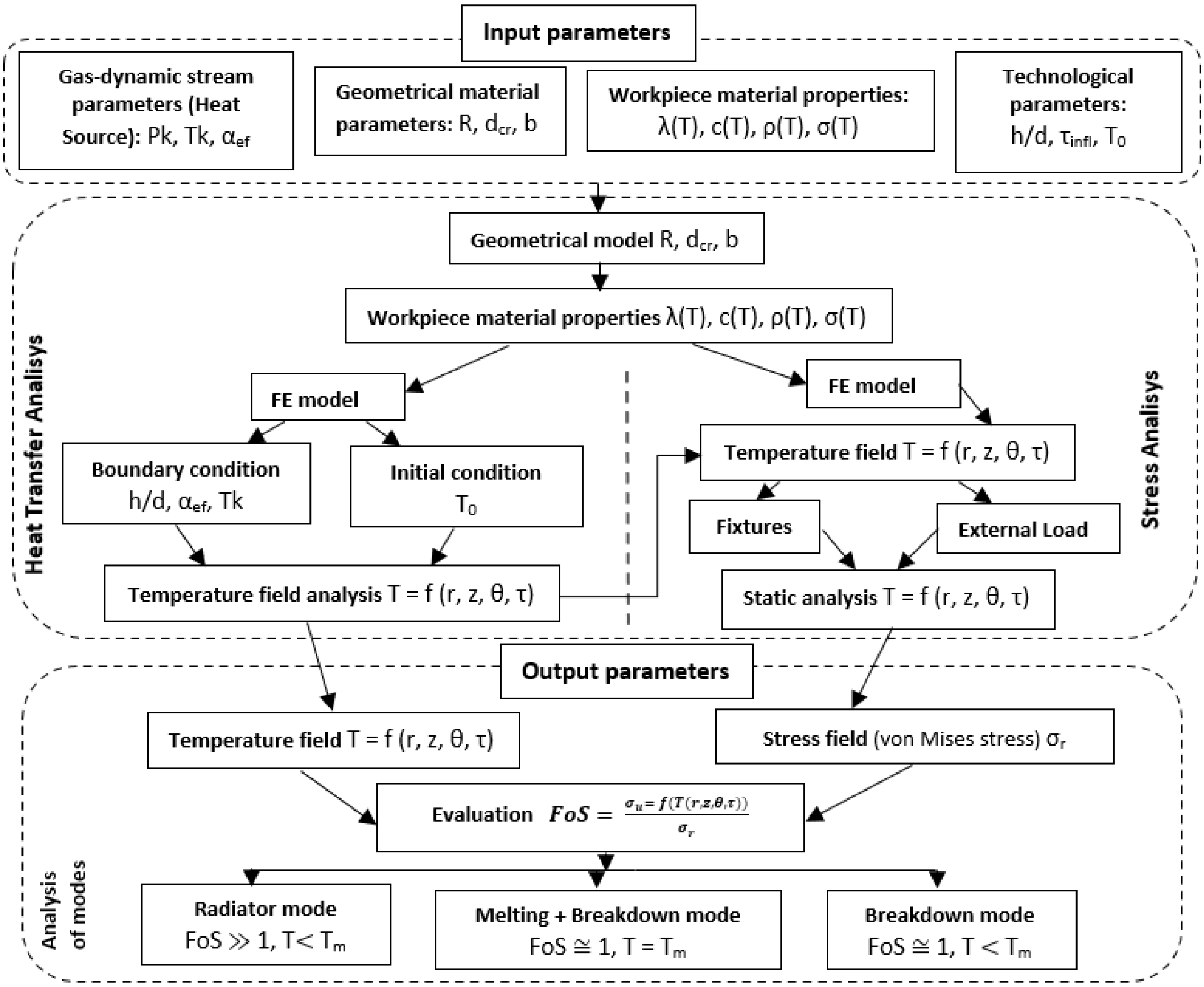

Figure 3: Flowchart of the algorithm for investigating the cutting of sheet materials by a supersonic high - temperature jet

The presented flowchart illustrates the structure and sequence of the numerical model developed to analyze the processes of supersonic high-temperature gas jet interaction with a plate. The input parameters for the modeling include the gas-dynamic characteristics of the jet (combustion chamber pressure P_k, combustion chamber temperature T_k, and heat transfer coefficient α_{ef}, the geometric properties of the plate (fixation radius R, jet diameter at the point of contact with the plate d_{str}, and plate thickness b), as well as the plate's thermophysical and mechanical properties, represented by temperature-dependent functions of thermal conductivity $\lambda(T)$, specific heat capacity $c(T)$, density $\rho(T)$, and tensile strength $\sigma(T)$.

DOI: 10.13009/EUCASS2025-270

Additionally, the model accounts for technological process parameters such as the dimensionless distance between the nozzle and the plate surface ($h\, d_n^{-1}$), the jet diameter at the impact point (d_{str}), the jet exposure time (τ_{inf}), and the initial temperature of the plate material (T_0).
Based on the specified input parameters, a geometric model is created, followed by a heat transfer analysis and a stress analysis. The heat transfer analysis is based on finite element modeling, which accounts for the initial and boundary conditions, namely the thermal impact of the jet and the initial temperature of the plate. The outcome of the heat transfer analysis is the temperature field $T = f(r, z, \theta, \tau)$, allowing the temperature at any point within the plate to be determined at any moment during the jet exposure time τ_{inf}.
The stress analysis is also conducted using the finite element method, with the temperature field obtained from the heat transfer analysis serving as input data. Boundary conditions are applied to the model, along with an external load corresponding to the dynamic pressure exerted by the jet. As a result of the simulation, stress fields are determined, particularly the von Mises equivalent stress σ_r.
The results of the heat transfer and stress analyses are integrated into a final criterion for evaluating the plate's structural state: the Factor of Safety (FoS), calculated as the ratio of the temperature-dependent tensile strength of the material to the acting stresses. This criterion, combined with the temperature field, enables the identification of three characteristic modes of jet–material interaction:

- radiator mode, where the Factor of Safety exceeds one (FoS $\gg$ 1), and the plate undergoes heating without reaching the melting temperature ($T < T_m$);
- melting + breakdown mode, where the Factor of Safety approaches unity (FoS $\cong$ 1) and the surface temperature reaches the melting point ($T = T_m$);
- breakdown mode, characterized by a Factor of Safety less than or equal to one (FoS $\cong$ 1), where material failure occurs before the melting temperature is reached ($T < T_m$) due to a combination of thermal weakening and dynamic jet loading.

Thus, the proposed flowchart describes the structure and sequence of the numerical investigation of the cutting process of plates by a supersonic high-temperature jet and enables a comprehensive assessment of the influence of jet parameters and plate material properties on the efficiency of the fragmentation process.
In the present study, aviation-grade aluminum alloys were selected as the plate material due to their widespread use in aerospace structures. These materials are known for their high strength-to-weight ratio, good corrosion resistance, and excellent technological properties (Table 1). The selection of these alloys is substantiated in [1].

Table 1: Nominal composition of alloying elements (wt%)

	Cu	Mn	Mg	Zn	Cr	Al	MetallSystem
2024	3.8 – 4.9	0.3 – 0.9	1.2 – 1.8	0.25 max	0.1 max	rem	AlCuMg2
	Others **Fe** 0.5 max						
7075	1.2 – 2.0	0.3 max	2.1 – 2.9	5.1 – 6.1	0.18 – 0.35	rem	AlZnMgCu1,5
	Others **Fe** 0.5 max; **Ti** 0.2 max						
2219	5.8 – 6.8	0.2 – 0.4	0.02 max			rem	AlCu
	Others **Fe** 0.3 max; **V** 0.05 – 0.15; **Zr** 0.05 – 0.15						
2124	3.8 – 4.9	0.3 – 0.9	1.2 – 1.8	До 0.25		rem	AlCuMg
	Others **Fe** 0,5 max; **Ti** 0,15 max; **Si** 0,5 max						

To simulate the thermal and force effects of high-speed jet interaction with the plate, the following assumptions were made:

1. The plate material is homogeneous and isotropic, with physical and mechanical properties dependent on temperature.
2. The jet impact at an orthogonal encounter forms a circular contact area with radius r_{cr}.
3. Both the gas-dynamic (force) and thermal effects are uniformly distributed within this contact area.
4. The distribution of heat in the thin, rigid plate is considered complete within radius R.
5. Thermal radiation losses in the cutting zone are neglected.

In accordance with these assumptions, modeling was performed using the following geometric parameters: r = 9 mm, R = 108 mm, and plate thickness b = (2–10) mm. The material properties as functions of temperature, including thermal conductivity (λ), specific heat capacity (c), and density (ρ), ultimate strength (σ) were taken into account in the model. Table 2 shows the temperature dependence material properties as functions of temperature. The properties of the 2124 alloy are described in detail in [2].

Table 2: Properties of Aluminium Alloys [13]

Temp. (°K)	**Thermal_Conductivity, (W m^{-1} K^{-1})**			**Specific_Heat, (J kg^{-1} K^{-1})**			**Density, (kg m^{-3})**			**Ultimate strength, (MPa)**		
	2024 T3	**7075 T6**	**2219**	**2024 T3**	**7075 T6**	**2219**	**2024 T3**	**7075 T6**	**2219**	**2024 T3**	**7075 T6**	**2219**
273	100	130	123	896	835	840	2823	2810	2830	485	570	460
373	140	140	134	915	897	900	2754	2805	2781	460	525	379
473	148	145	151	950	916	910	2705	2795	2760	380	315	277
573	155	147	159	952	974	960	2654	2790	2740	170	90	148
673	155	150	172	1080	1013	1010	2613	2787	2711	50	40	25
773	165	155	185	1100	1128	1060	2559	2783	2692	25	20	14
873	180	180	195	1150	1205	1080	2540	2777	2700	20	15	10

2.1 Modeling of Heat Source

Modeling of the heat source is a critical aspect of the analysis of the cutting process using supersonic jets. The heat source is schematically presented in Figure 1(b). This schematic illustrates the quasi-uniform distribution of jet parameters (pressure, temperature, and velocity) within the first Mach barrel region, which is critical for accurately modeling the thermal and mechanical loading on the plate near the stagnation point.
The primary parameters determining the intensity of the thermal impact include the combustion chamber pressure (P_k), the combustion products temperature (T_k), the nozzle exit diameter (d_n), the mass flow rate of the combustion products, and the heat transfer coefficient (α_{ef}). In the modeling, it is assumed that the optimal conditions for achieving the maximum thermal and dynamic effects of the jet are realized within the region of the first Mach barrel, corresponding approximately to (1.5–2) d_n.
Upon impingement on the plate surface, the jet flow decelerates, and its kinetic energy is converted into thermal energy. In the contact zone between the jet and the plate, the recovered parameters are assumed to be approximately equal to the stagnation values: $T_s{*} \approx T_k{*}$ and $P_s{*} \approx P_k{*}$. The heat flux q_w from the jet to the plate is described by Newton's law of cooling:

$$q_w = \alpha_{ef}\,(T_s - T), \qquad \textbf{(2)}$$

where q_w – specific heat flux from the combustion products jet to the plate, W m^{-2};
α_{ef} – heat transfer coefficient, W m^{-2} K^{-1};
T_s – jet temperature at the plate surface, K;
T – initial temperature of the plate, K.
In this study, it was assumed that both the heat flux q_w and the heat transfer coefficient α_{ef} are uniformly distributed over the jet impact area on the plate surface.
For the calculations, the parameters of a low-thrust rocket engine operating on a compressed air and hydrocarbon fuel mixture with an oxidizer-to-fuel ratio of 1.15–1.2 were used [2]. The main characteristics of the engine are presented in Table 3. The experimental results of using cutting tools with these and others parameters are presented in detail in [2].

Table 3: Main parameters of the low-thrust rocket engine

Cutting tool	Combustion chamber pressure, **P_k, МПа**	Temperature in the combustion chamber, **$T_к$, К**	Heat transfer coefficient, **h, W m^{-2} K^{-1}**	Heat flow, **q_w, Вт м$^{-2}$**	Mass fuel consumption, **m_f, kg s^{-1}**	Thermogasdynamic parameter, **m_f P_k, kg s^{-1} Pa**
1	0.6	2105.96	6969.69	$1.264\cdot10^{7}$	0.034	$2.02\cdot10^{4}$
2	1.1	2108	12775	$2.319\cdot10^{7}$	0.24	$2.64\cdot10^{5}$

DOI: 10.13009/EUCASS2025-270

2.2 Heat Transfer Analysis

The heat transfer in the model is described based on the fundamental principles of Fourier's law of heat conduction:

$$\frac{\partial T}{\partial \tau} = \frac{1}{c \cdot \rho} div(\lambda \cdot gradT) + \frac{q_v}{c \cdot \rho}, \quad (3)$$

where c, ρ, λ – the thermophysical properties of the barrier material, dependent on the metal's temperature.
Since there is no internal heat source, the equation simplifies to:

$$\frac{\partial T}{\partial \tau} = \frac{1}{c\rho}\left(\frac{\partial}{\partial r}\left(\lambda \frac{\partial T}{\partial r}\right) + \frac{\lambda}{r}\frac{\partial T}{\partial r} + \frac{\partial}{\partial z}\left(\lambda \frac{\partial T}{\partial z}\right)\right) \quad (4)$$

The thermal processes in the material were analyzed in two stages: heating to the melting temperature and the subsequent melting.

$$\text{At } T < T_m \begin{cases} c \cdot \rho \frac{\partial T}{\partial \tau} = \frac{1}{r}\frac{\partial (r\lambda \frac{\partial T}{\partial r})}{\partial r} + \frac{\partial (\lambda \frac{\partial T}{\partial z})}{\partial z} \\ \frac{\partial V}{\partial \tau} = 0 \end{cases}; \qquad \text{at } T = T_m \begin{cases} L_m \cdot \rho \frac{\partial V}{\partial \tau} = \left(\frac{1}{r}\frac{\partial (r\lambda \frac{\partial T}{\partial r})}{\partial r} + \frac{\partial (\lambda \frac{\partial T}{\partial z})}{\partial z}\right) \cdot dV \\ \frac{\partial T}{\partial \tau} = 0 \end{cases}, \quad (5)$$

The boundary conditions were determined, which, together with the differential equations, provide a complete mathematical description of the heat conduction process:

– $T(r,z,0) = T_0$ for (r,z) ϵ D – initial condition (first kind boundary condition);
– $q_{w\ z = 0,\ rc < r \leq R\ u\ z = b} = 0$ – second kind boundary condition (adiabatic surface outside the jet impact zone);
– $q_{w\ z = 0,\ r \leq rc} = \alpha_{ef}(T_s - T)$ – third kind boundary condition (convective heat transfer at the jet impact zone).

To obtain the temperature field distribution within the plate, a series of finite element simulations was performed, covering various jet impact regimes and parameter ranges (see Fig. 4). The simulations enabled the investigation of the temperature evolution at different stages of jet exposure, as well as the characterization of the temperature gradient variations across the plate thickness and along the radial direction.

2.3 Stress Analysis

To determine the maximum stresses in the plate, it was modeled as an axisymmetrically loaded, rigid circular plate, fixed along the radius R (see Fig. 1). The evaluation of the stress-strain state and the strength of the plate, taking into account the temperature-dependent material properties, constitutes a statically indeterminate problem within the framework of axisymmetric plate bending theory. The fundamental equations incorporate the principles of statics, the geometric characteristics of the plate, and the temperature-dependent material behavior in accordance with classical engineering plate theory. A qualitative representation of the stress distribution $\sigma_r(r)$ is shown in Fig. 4.

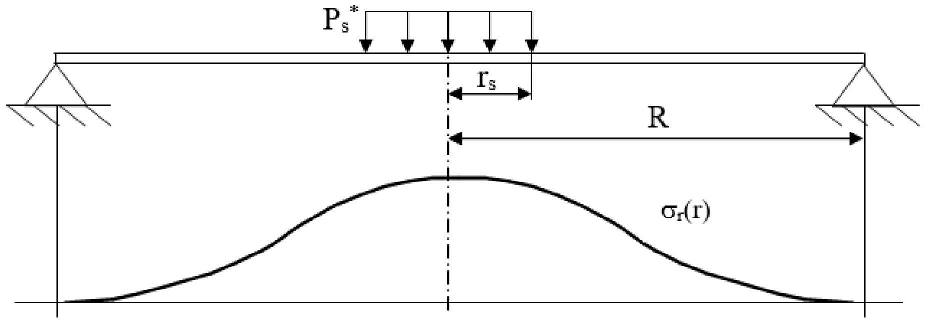

Figure 4: Qualitative representation of the stress distribution

The time required to satisfy the breakdown condition [see Eq. (1) above] corresponds to the duration necessary for the realization of the combined thermal and mechanical effects of the supersonic high-temperature combustion jet within the plate material. The results obtained in Sections 2.2 and 2.3 provide the basis for determining the moment at which the breakdown condition is achieved.

DOI: 10.13009/EUCASS2025-270

3. Finite element simulation

Numerical modeling of the described interaction process was conducted using the SolidWorks Simulation finite element software. Temperature-dependent thermal and mechanical properties of selected aluminum alloys (see Table 2), were implemented through the creation of custom-defined material models within SolidWorks. The operating parameters of the supersonic hot gas jet cutting tool utilized in simulations are presented in Table 1.
The simulation model was developed based on the assumptions and limitations outlined earlier, as well as on the application of Fourier's law of heat conduction and classical engineering plate theory, enabling verification of the validity of the breakdown condition [see Eq. (1) above]. In this model, the cutting tool acts axisymmetrically on a circular aluminum plate, which is rigidly clamped along its outer edge (see Fig. 5). The effect of thermal expansion was excluded from the analysis, justified by its negligible impact considering the brief jet exposure duration and the plate's geometric dimensions.

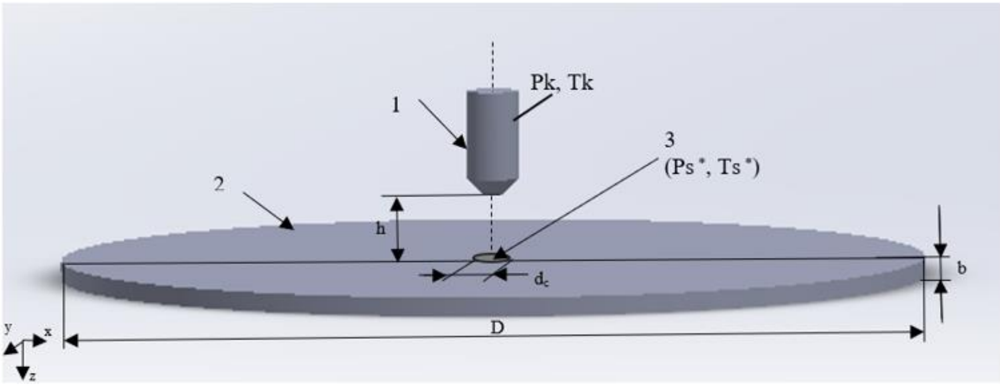

1 – nozzle;
2 – plate;
3 – stagnation point;
P_k, T_k – combustion chamber parameters;
P_s^*, T_s^* – stagnation parameters

Figure 5: Model of the fragmentation process

To accurately describe the transient evolution of temperature fields within the plate, a time-dependent thermal analysis was performed using a defined temporal discretization. Although the implementation of transient analysis significantly increased computational demands, it ensured precise characterization of temperature distributions at arbitrary locations and times within the model domain, expressed mathematically as $T = f(r, z, \tau)$.
Subsequently, based on the results of the coupled thermal–mechanical simulations, the Factor of Safety (FoS) was evaluated at each finite element node for discrete time increments. The FoS, defined as the ratio between the temperature-dependent ultimate tensile strength of the material and the local von Mises equivalent stress, provides a quantitative, dimensionless measure of structural integrity under combined thermal and mechanical loading conditions. The calculation of FoS was performed according to the following relation:

$$FOS = \frac{\sigma_u = f(T(r,z,\tau))}{\sigma_r}. \quad \textbf{(6)}$$

The finite element mesh was composed of tetrahedral elements. A standard mesh convergence analysis was performed to determine the optimal element size, with the mesh being progressively refined by reducing the element dimensions from 1.5 mm down to 0.5 mm. Refinement continued until the maximum von Mises equivalent stress converged within a 5% change threshold across all elements. As a result, the final mesh had an element size ranging from 1.0 mm to 0.05 mm (see Fig. 6). Quality verification of the finite-element model revealed no critical errors, ensuring the reliability and accuracy of the simulation results.

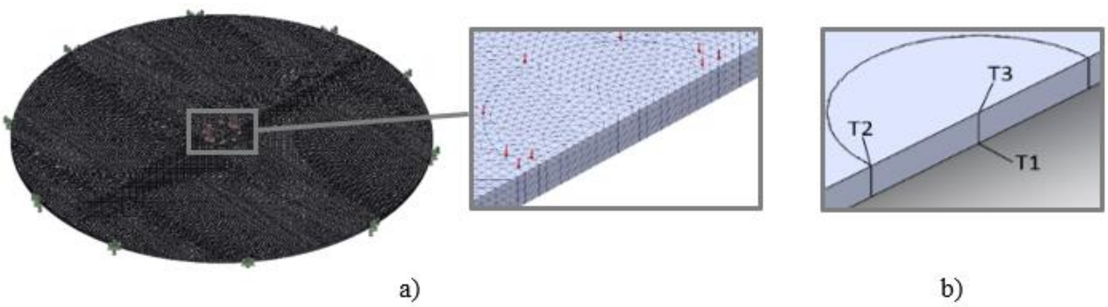

Figure 6: Simulation model: a) applying a mesh to a model; b) key points for testing parameters

DOI: 10.13009/EUCASS2025-270

In Fig. 6, the locations of three key points, T1, T2, and T3, are schematically indicated, where the results of thermal and stress analyses were monitored. Points T1 and T3 are aligned along the axis of the jet impact: T3 is located at the jet's point of incidence on the material's surface, while T1 is positioned on the rear surface, opposite to the impact site. Point T1 corresponds to location A (see Fig.1), where the breakdown condition [see Eq. (1) above] was expected to be satisfied. Monitoring the temperature evolution at T3 allowed the control of surface temperature to detect the onset of melting. Additionally, point T2 was positioned at the boundary of the jet's influence zone and was used to monitor parameters for a more detailed understanding of the heat transfer and stress distribution processes.

4. Results and Discussion

The results of the finite element simulations are presented and analyzed in this section. Particular attention is given to the distribution of temperature, the development of stress fields, and the assessment of material failure conditions under the influence of a supersonic high-temperature jet.

4.1 Temperature Distribution

Figure 7 illustrates a number of results from the thermal analysis. The samples, differing in thickness, were positioned at a distance from the nozzle corresponding to a dimensionless ratio $h\ d_n^{-1}$ = (1,5 ... 2), with the jet exposure time τ indicated for each case.

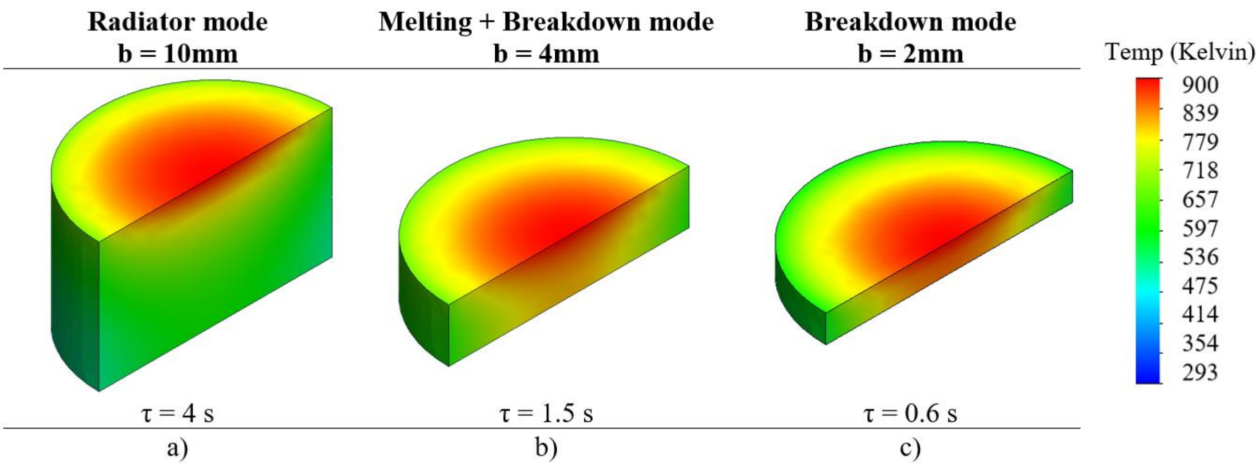

Figure 7: Temperature distribution through the material thickness obtained from SolidWorks Simulation (P_k = 0.6 MPa, plate material: 2024-T3): a) b = 10 mm, radiator mode; b) b = 4 mm, melting + breakdown mode; c) b = 2 mm, breakdown mode

The simulation results presented in Figure 7 illustrate the temperature distribution across the thickness of aluminum samples subjected to a supersonic high-temperature jet. Different interaction regimes are observed depending on the material thickness.

For the thickest sample with b = 10 mm (Fig. 7(a)), corresponding to the Radiator Mode, the temperature rises but does not reach the melting point even after prolonged exposure, due to the high thermal conductivity of the aluminum alloy. For the intermediate thickness b = 4 mm (Fig. 7(b)), the Melting + Breakdown Mode is identified, where surface melting initiates, followed by mechanical failure. In the case of the thinnest sample with b = 2 mm (Fig. 7(c)), the breakdown mode is realized, characterized by material failure before the surface reaches the melting temperature.

The maximum temperature is consistently achieved at the material surface along the jet axis, with the temperature decreasing radially outward from the center. These results confirm the thermal response predicted by the simulation model and support the classification of jet-material interaction regimes based on material thickness and exposure time.

4.2 Stress Distribution

The results of the stress analysis are presented in this section. Figure 8 illustrates the von Mises equivalent stress (σ_r) distribution induced by the dynamic component of the supersonic jet. The stress fields exhibit symmetry relative to the mid-plane of the plate, which is characteristic of axisymmetric loading conditions. It is observed that the magnitude of internal stresses remains largely unaffected by the duration of jet exposure, being primarily determined by the

DOI: 10.13009/EUCASS2025-270

magnitude of the applied dynamic load. Minor variations in stress contours, particularly near the material surface, are attributed to local mesh refinement and discretization effects. A mesh sensitivity analysis confirmed that these variations lie within acceptable engineering margins and do not influence the validity of the simulation results.

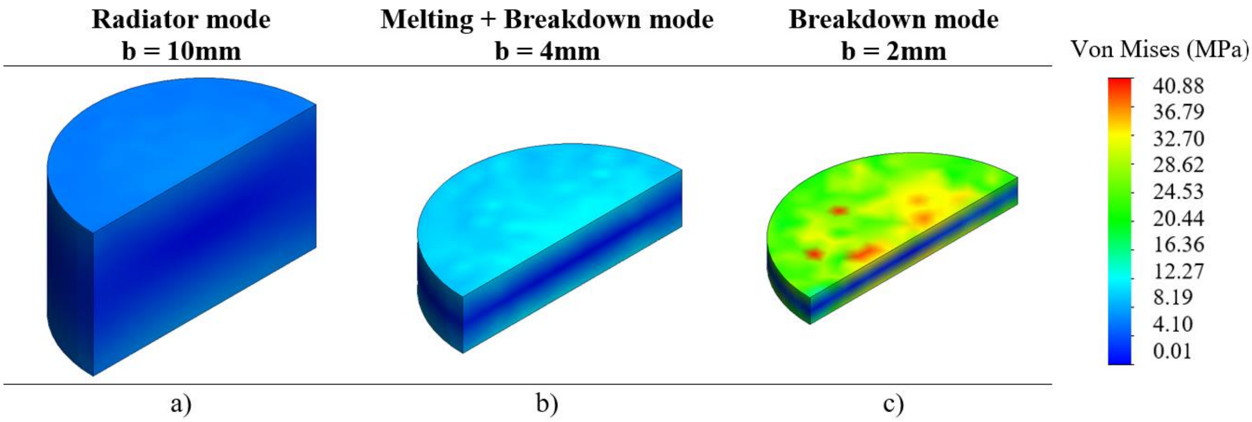

Figure 8: Distribution of internal stresses across the material thickness based on SolidWorks Simulation results (P_k = 0.6 MPa, plate material: 2024-T3): a) b = 10 mm, radiator mode, b) b = 4 mm, melting + breakdown mode, c) b = 2 mm, breakdown mode

4.3 Factor of Safety of the Material

Figure 9 illustrates the distribution of the Factor of Safety (FoS) across the material. The Factor of Safety (FoS) indicates how many times the ultimate load exceeds the actual applied load [see Eq. (6) above]. The numerical analysis confirms the division of the interaction zone into three distinct regions, each characterized by different mechanisms depending on the ratio between the thermogasdynamic parameter of the jet and the material thickness.

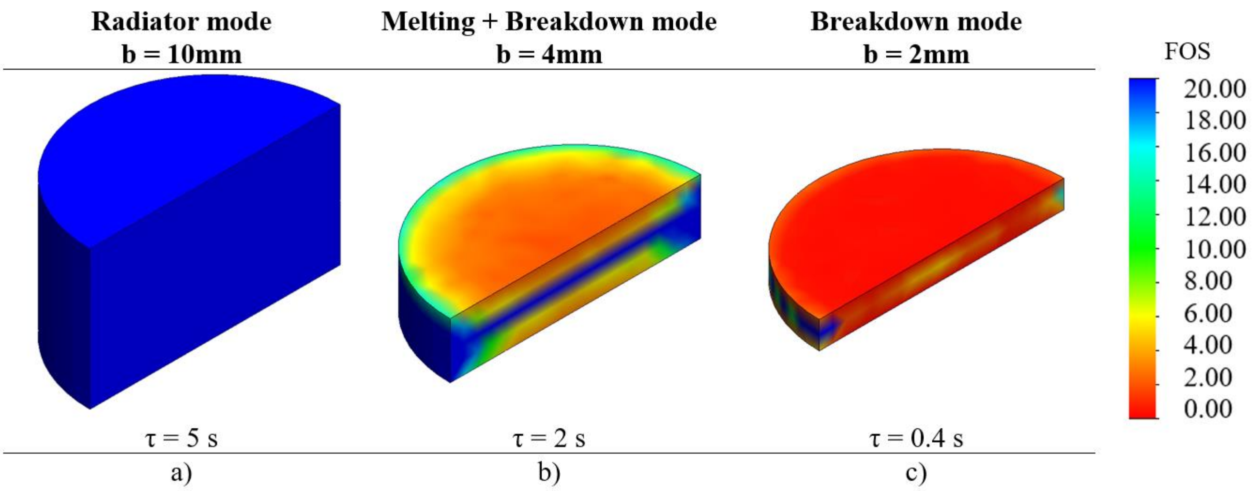

Figure 9: Factor of Safety distribution in the material based on SolidWorks Simulation results (Pk = 0.6 MPa, plate material: 2024-T3): a) b = 10 mm, radiator mode b) b = 4 mm, melting + breakdown mode, c) b = 2 mm, breakdown mode

For the sample with b = 10 mm, over 4 seconds of jet exposure, a gradual temperature redistribution occurs across the material thickness. The surface temperature gradient increases slowly, indicating that the thermal energy imparted by the jet is dissipated throughout the material. This cutting regime is referred to as the radiator mode – a zone where the heat delivered by the jet is distributed without causing material damage, and where even prolonged thermal exposure of the plate occurs without loss of structural integrity. Such a cutting mode is ineffective for fragmenting 10 mm thick aluminum alloys, as the supplied energy is insufficient to initiate material failure.
For the 4 mm thick sample, after 1.5 seconds, surface melting begins at the jet impact side (see Fig. 7(b)). By 2 seconds, as shown in Fig. 9(b), the breakdown condition [see Eq. (1) above] is still not satisfied. However, as melting progresses at the surface, the thickness of the unmelted material decreases, and eventually the breakdown condition is achieved,

DOI: 10.13009/EUCASS2025-270

despite the occurrence of surface melting. This regime is referred to as melting+breakdown mode – a zone where localized surface melting initiated by the jet is followed by mechanical fragmentation and ejection of material from the cut zone. In this mode, the time to reach the melting temperature along the jet axis is shorter than the time required to satisfy the breakdown condition.
For the 2 mm thick sample, the temperature at the jet impact point rapidly reaches the melting temperature (after approximately $\tau = 0.6$ s, see Fig. 7(c)). However, as early as 0.4 seconds after the start of jet action, the FoS at point T1 falls below 1 (see Fig. 9(c)). This indicates that the breakdown condition [see Eq. (1) above] is fulfilled on the rear side of the plate before the surface temperature reaches the melting point. Thus, the breakdown mode is realized – a regime in which structural failure occurs due to a combination of dynamic impact and thermal weakening, without melting of the material in the cutting zone. In this mode, the time required to satisfy the breakdown condition is shorter than the time needed to initiate melting along the jet axis on the upper surface of the plate.
Figure 10 presents the graphical implementation of the most energy-efficient Breakdown Mode, providing confirmation of the assumptions discussed earlier.

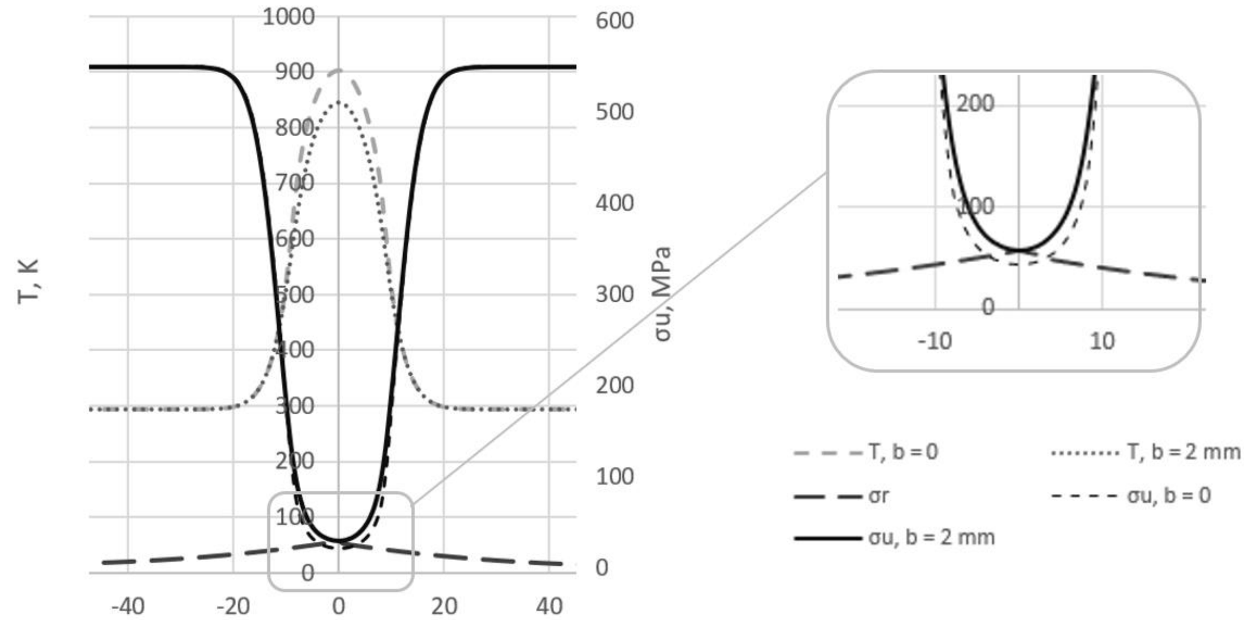

Figure 10: Breakdown mode: graph based on simulation data

The graph presents the radial distribution of temperature and stress across the top and bottom surfaces of the aluminum plate under jet exposure. The temperature at the top surface (T, b = 0) peaks at approximately 900 K near the jet axis (r = 0), while the bottom surface (T, b = 2 mm) also shows significant heating, reaching around 830 K. The von Mises stress distribution (σr) and surface stresses (σu, b = 0; σu, b = 2 mm) exhibit pronounced peaks near the center, reflecting the localized thermal and mechanical loading conditions. The trend line indicates the region where the breakdown condition is met, confirming the expected thermal and mechanical behavior characteristic of the Breakdown Mode.

4.4 Validation of Simulation Results

To verify the predictive accuracy of the numerical model, simulation outcomes were compared with experimental data for 2124 aluminum alloy plates under equivalent thermogasdynamic conditions [2]. Specifically, the jet exposure times required to initiate material breakdown were used as benchmark values.
Table 4 presents a comparison between experimental and simulated breakdown times for plates of different thicknesses under a fixed jet parameter ($m_f\,P_k = 0.2.\cdot 10^5$ kg s^{-1} Pa). As shown in Table 4, the scatter in experimental results may be attributed to the inherent complexity of capturing accurate measurements under transient high-temperature jet conditions, combined with uncertainties related to jet stability, surface state, and material variability.
The discrepancies in simulation results may be attributed to challenges in accurately defining the boundary conditions. In addition, deviations could stem from variability in the material properties, since the simulation was based on tabulated values, whereas the actual material may have differed due to factors such as thermal treatment or manufacturing variations. The observed deviations lie within the range of 37–41 %, which is acceptable for transient coupled thermal–mechanical problems involving dynamic jet loading and temperature-dependent material behavior.

DOI: 10.13009/EUCASS2025-270

Similar levels of deviation have been reported in related studies [14–15], supporting the predictive adequacy of the proposed model. For thicker plates (b = 6 mm), breakdown was not observed experimentally within the 5-second exposure limit, while the simulation predicted partial damage initiation. This time constraint was imposed due to economic and resource limitations in conducting prolonged high-temperature experiments.

Table 4: Comparison of experimental and simulated breakdown times

b, mm	Thermogasdynamic Parameter **m_f P_k, kg s^{-1} Pa**	Experimental Time, **τ, s**	Simulated Time, **τ, s**	Deviation, **%**
2	$0.2 \cdot 10^5$	0.75 ± 0.25	0.42	41
3	$0.2 \cdot 10^5$	1.35 ± 0.3	0.85	37
4	$0.2 \cdot 10^5$	3.04 ± 0.2	1.8	40
6	$0.2 \cdot 10^5$	> 5	2.7	*

* Breakdown not observed within time limit

Overall, the validation confirms that the developed numerical model adequately captures the key mechanisms of material failure under supersonic jet impact and can be used for further optimization of cutting parameters and adaptation to various operating regimes. Future work will focus on refining the model by improving boundary condition definitions and incorporating more accurate material data. In addition, further experimental studies are planned to enhance the reliability of the model and provide a more robust basis for predictive calculations.

4.5 Summary of results

Figures 11 and 12 summarize the simulation results obtained across 32 scenarios. In Figure 11 the Y-axis represents the jet exposure time required to affect the material, while the X-axis shows the thermogasdynamic parameter mf Pk. This parameter was introduced for the first time as a key characteristic in the study of thermo-gas-jet devices. Unlike conventional flow-based characteristics of similar systems, it accounts not only for the thermal effect but also for the dynamic (force) impact of high-temperature supersonic gas jets on the plate. This approach enabled the differentiation and systematization of various interaction modes between supersonic jets and plates [2].
Based on the simulation results, three characteristic modes of jet–material interaction were identified: radiator mode, melting + breakdown mode, and breakdown mode.
Figure 12 presents the qualitative assessment of the breakdown phenomenon for averaged thicknesses of aerospace aluminum alloys. In the figure, different colors indicate regions distinguished by internal process mechanisms.
As shown in Figure 12, cutting tool 1 (m_f $P_k = 2.02 \cdot 10^4$ kg s^{-1} Pa, see Table 3 above) achieves material perforation for samples with thicknesses of 2–3 mm, occurring within 0.5 to 1 second after the onset of jet impact. For thicker samples, surface melting initiated before perforation, leading to hole formation after 1–2 seconds of exposure. In the case of cutting tool 2 (m_f $P_k = 2.64 \cdot 10^5$ kg s^{-1} Pa, see Table 3 above), the jet possesses higher energy, resulting in more intensive heat transfer processes. Direct perforation was observed for 2 mm thick samples, while for thicker materials, surface melting preceded the mechanical breakdown.

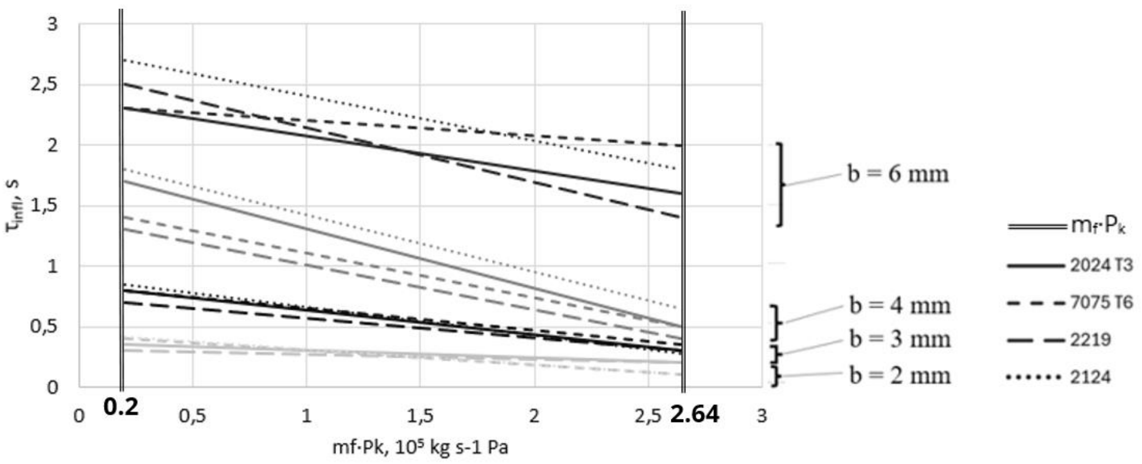

Figure 11: Simulation results: breakdown time as a function of thermogasdynamic parameter m_f P_k for various plate thicknesses: cutting tool 1 m_f $P_k = 0.2. \cdot 10^5$ kg s^{-1} Pa; cutting tool 2 m_f $P_k = 2.64 \cdot 10^5$ kg s^{-1} Pa

DOI: 10.13009/EUCASS2025-270

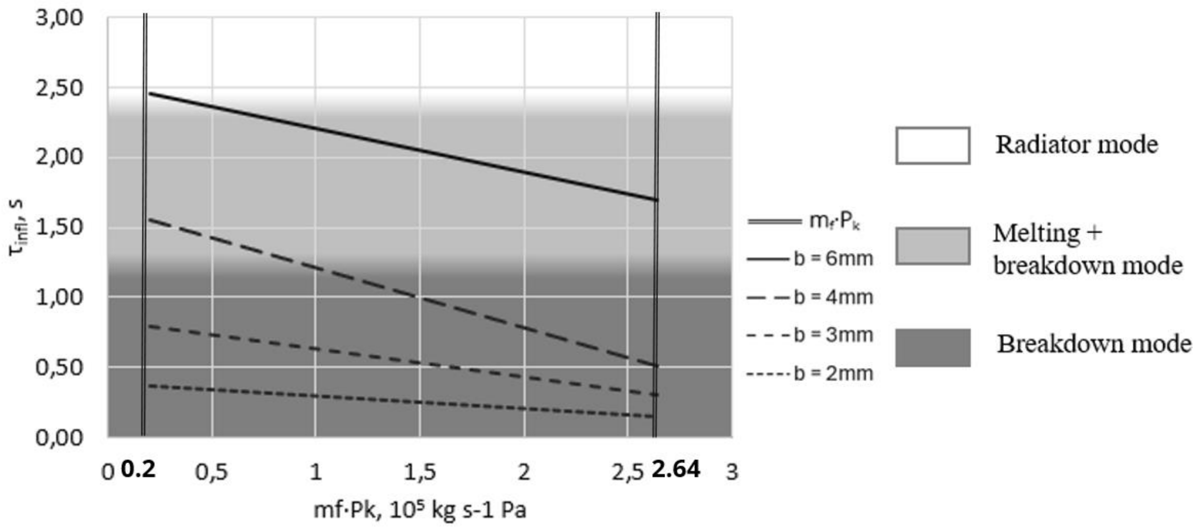

Figure 12: Qualitative representation of simulation results for averaged data of aluminum alloys, highlighting different failure mechanisms

The analysis of simulation results presented in Figures 11 and 12 reveals several consistent patterns in how the thermogasdynamic parameter influences the jet–material interaction. These observations not only confirm the predictive capabilities of the proposed model but also provide physical insight into the underlying mechanisms of failure initiation and propagation. Based on this, several general trends can be identified:

- The breakdown time τ_{br} is primarily affected by the combustion chamber pressure, the mass flow rate of the jet, and the plate thickness;
- For plates of the same thickness, the breakdown time is most accurately characterized by the thermogasdynamic parameter m_f P_k. As m_f P_k increases, τ_{br} decreases in a nonlinear manner. It was also established that achieving material breakdown requires a specific value of the thermogasdynamic parameter m_f P_k, which can be attained through different combinations of chamber pressure P_k and nozzle throat diameter d_{kr}. This observation highlights the possibility of selecting appropriate jet parameters to achieve the desired effect without relying solely on increasing pressure.
- For a given plate thickness**,** there exists a specific value of the thermogasdynamic parameter beyond which further increases result in only minor changes in breakdown time. It is evident that with increasing m_f P_k, the breakdown time will asymptotically approach the horizontal axis, which is consistent with the experimental observations reported in [2]. This suggests that thermal input becomes less influential, and the failure process is increasingly governed by internal stress fields and material microstructure.

The study confirmed that a supersonic exhaust jet from a rocket engine possesses sufficient concentrated energy to fragment aluminum sheet materials without requiring full melting, and that this effect can be effectively utilized for cutting the structures of decommissioned aerospace vehicles.

The present study complements previous research on the fragmentation processes of aluminum alloys. Investigations by Zabotin et al. [14] and Sharma et al. [15] primarily focus on melting-based cutting modes. Zabotin et al. [14] examined the cutting of aluminum sheet materials with high thermal conductivity using transonic jets from oxygen-hydrogen and oxygen-propane combustion-jet cutting devices, deriving an empirical relationship for cutting speed based on the time required for the formation of a hole by melting**.**

It should be noted that, despite differences in cutting tool parameters, the initial assumptions regarding the formation of the cut zone by a supersonic jet are confirmed, as the results obtained are consistent with those reported by Zabotin et al. [14] for melting-based cutting. In his case, melting-based cutting required significantly more energy compared to breakdown-based cutting**,** since the heat had to first raise the material to the melting temperature and then induce melting [16]. In contrast, breakdown-based cutting achieves material failure primarily through dynamic loading and localized thermal weakening, making it a more energy-efficient process.

Sharma et al. [15] modeled laser cutting of the Al-2024 aluminum alloy in ANSYS. Both studies support the assumption of material homogeneity and isotropy, as well as the assumption that the jet–material contact area during orthogonal impingement is circular. In [15], the non-uniform distribution of heat intensity across the beam cross-section, characteristic of laser cutting, is considered and described using a Gaussian distribution. In contrast, the present study assumes a uniform distribution of thermal characteristics across the jet cross-section.

The literature review, combined with the numerical modeling of orthogonal jet-plate interaction, identified key parameters influencing the cutting process: thermal, physical, and geometric properties of the material; initial process conditions; thermogasdynamic characteristics of the jet; the dimensionless distance $h\ d_n^{-1}$; and the wave structure of

DOI: 10.13009/EUCASS2025-270

the jet, as noted by Jiang et al. [3] and Chan et al. [4]. In these publications, acoustic effects were considered significant, which is primarily attributed to the larger scales of the investigated objects. For small-thrust engines, however, acoustic effects have a negligible influence on the fragmentation process.

The results obtained in this study provide a deeper understanding of the mechanisms governing the interaction of supersonic jets with materials and can be used to further improve cutting and disposal technologies for metallic structures made of various materials, both in terrestrial and extraterrestrial environments. Importantly, unlike previous studies focused on melting-based cutting, the present work demonstrates the potential of energy-efficient fragmentation driven by dynamic effects without the need for complete material melting. This opens new opportunities for the development of advanced, low-energy cutting methods suitable for aerospace structure dismantling, debris mitigation, and material processing under extreme conditions.

Conclusion

This study presents a finite element model for the orthogonal cutting of aluminum alloys by a supersonic, high-temperature gas jet generated by a low-thrust rocket engine. The model accounts for both the thermal and mechanical effects of the jet, incorporating the temperature-dependent thermophysical properties of the material.

The analysis revealed three distinct modes of jet–material interaction:

1. Radiator mode – where heat dissipates without causing material failure;
2. Melting + breakdown mode – where surface melting initiates before structural failure;
3. Breakdown mode **–** where material failure occurs through dynamic pressure and localized thermal weakening, without reaching the melting point.

Importantly, the breakdown mode demonstrated a significant energy-saving potential, reducing the energy requirement for cutting by approximately 20% compared to melting-based approaches [2]. The modeling outcomes identified critical zones of temperature and stress concentration, confirming that material failure is driven by localized thermal weakening and dynamic impact forces. The results are consistent with and extend previous studies focused on melting-based cutting (Zabotin et al., Sharma et al.), while proposing a novel, non-melting fragmentation mechanism for high-conductivity materials. The developed model provides a basis for optimizing cutting parameters for aluminum alloys and can be further adapted for cutting a broader range of materials, including titanium alloys, steels, and composites.

Future work will focus on refining the finite element model and expanding its application to various jet configurations, including different geometric parameters of low-thrust rocket engines and alternative fuel compositions, effectively leading to the development of new types of cutting tools. Additionally, it is planned to adapt the modeling approach for operation in extraterrestrial environments, particularly under lunar conditions, in alignment with In-Situ Resource Utilization (ISRU) strategies. The results of this study provide a foundation for advancing sustainable, low-energy material processing technologies for both terrestrial applications and future space exploration initiatives.

References

[1] Nabokina, T., and Bach, C. 2024. Assessing the applicability of terrestrial recycling fragmentation technologies in lunar conditions. In: Pavlikov, V., and Krytskyi, D. (Eds.), Integrated Computer Technologies in Mechanical Engineering – 2024. ICTM 2024. Lecture Notes in Networks and Systems. Springer, Cham. (in press).

[2] Nabokina, T. 2013. Cutting of metal by supersonic high-temperature gas streams with unhardening effect. Dissertation, Kharkiv Aviation Institute, Kharkiv, Ukraine.

[3] Jiang, C., Han, T., Gao, Z., and Lee, C.-H. 2019. A review of impinging jets during rocket launching. Progress in Aerospace Sciences, 109, 100547. https://doi.org/10.1016/j.paerosci.2019.05.007

[4] Chan, L., Chin, C., Soria, J., and Ooi, A. 2014. Large eddy simulation and Reynolds-averaged Navier-Stokes calculations of supersonic impinging jets at varying nozzle-to-wall distances and impinging angles. Int. J. Heat Fluid Flow, 47, 31–41. https://doi.org/10.1016/j.ijheatfluidflow.2014.02.005

[5] Goldstein, R. J., and Franchett, M. E. 1988. Heat transfer from a flat surface to an oblique impinging jet. ASME Journal of Heat Transfer, 110(1), 84–90. https://doi.org/10.1115/1.3250477

[6] Dairay, T., Fortuné, V., Lamballais, E., and Brizzi, L.-E. 2015. Direct numerical simulation of a turbulent jet impinging on a heated wall. J. Fluid Mechanics, 764, 362–394. https://doi:10.1017/jfm.2014.715

[7] Martin, H. 1977. Heat and mass transfer between impinging gas jets and solid surfaces. In: Hartnett, J.P., and Irvine, T.F. (Eds.), Advances in Heat Transfer, Vol. 13, Elsevier, pp. 1–60. https://doi.org/10.1016/S0065-2717(08)70221-1

[8] Zohbi, B. E., Hassan, M. E., Afyouni, N., Meraim, K. A., Sakout, A., and Assoum, H. H. 2024. A review on aero-acoustics and heat transfer in impinging jets. Int. J. Technology, 15(5), 1398–1419. https://doi.org/10.14716/ijtech.v15i5.7020

DOI: 10.13009/EUCASS2025-270

[9] Cooper, D., Jackson, D. C., Launder, B. E., and Liao, G. X. 1993. Impinging jet studies for turbulence model assessment – I. Flow-field experiments. Int. J. Heat Mass Transfer, 36(10), 2675–2684. https://doi.org/10.1016/S0017-9310(05)80204-2
[10] Ben Kalifa, R., Habli, S., Mahjoub Saïd, N., Bournot, H., and Le Palec, G. 2016. Parametric analysis of a round jet impingement on a heated plate. Int. J. Heat Fluid Flow, 57, 11–23. https://doi.org/10.1016/j.ijheatfluidflow.2015.11.005
[11] Vinze, R., Chandel, S., Limaye, M. D., and Prabhu, S. V. 2016. Influence of jet temperature and nozzle shape on the heat transfer distribution between a smooth plate and impinging air jets. Int. J. Thermal Sciences, 99, 136–151. https://doi.org/10.1016/j.ijthermalsci.2015.08.009
[12] Subramanian, S., Craig, B., White, C., Kontis, K., Evans, D., and Van den Eynde, J. 2024. Underexpanded jet impingement in near vacuum environment. Physics of Fluids, 36(10), 107104. https://doi.org/10.1063/5.0230314
[13] NASA. Materials and Processes Technical Information System (MAPTIS). NASA Marshall Space Flight Center. https://maptis.nasa.gov (accessed April 2025).
[14] Zabotin, V. G., Kosenko, A. I., Osipov, A. I., et al. 1983. Thermal mechanism of destruction of the barrier by a transonic jet of combustion products of rocket fuel. J. Eng. Physics, 44, 509–513. https://doi.org/10.1007/BF00831936
[15] Sharma, P., Dubey, A. K., and Pandey, A. K. 2014. Numerical study of temperature and stress fields in laser cutting of aluminium alloy sheet. Procedia Materials Science, 5, 1887–1896. https://doi.org/10.1016/j.mspro.2014.07.510
[16] Bychkov A. S., Kondratiev A. V. 2019. Criterion-based assessment of performance improvement for aircraft structural parts with thermal spray coatings. J. Superhard Materials, 41(1), 53–59. https://doi.org/10.3103/S1063457619010088